# Concurrent Tonotopic Processing Streams in Auditory Cortex

Charles C. Lee[1], Kazuo Imaizumi[2], Christoph E. Schreiner[2] and Jeffery A. Winer[1]

[1]Division of Neurobiology, Department of Molecular and Cell Biology, University of California, Berkeley, CA 94720-3200, USA and [2]Coleman Memorial Laboratory, W.M. Keck Center for Integrative Neuroscience, University of California, San Francisco, CA 94143-0732, USA

**The basis for multiple representations of equivalent frequency ranges in auditory cortex was studied with physiological and anatomical methods. Our goal was to trace the convergence of thalamic, commissural, and corticocortical information upon two tonotopic fields in the cat, the primary auditory cortex (AI) and the anterior auditory field (AAF). Both fields are among the first cortical levels of processing. After neurophysiological mapping of characteristic frequency, we injected different retrograde tracers at separate, frequency-matched loci in AI and AAF. We found differences in their projections that support the notion of largely segregated parallel processing streams in the auditory thalamus and cerebral cortex. In each field, ipsilateral cortical input amounts to ~70% of the number of cells projecting to an isofrequency domain, while commissural and thalamic sources are each ~15%. Labeled thalamic and cortical neurons were concentrated in tonotopically predicted regions and in smaller loci far from their spectrally predicted positions. The few double-labeled thalamic neurons (<2%) are consistent with the hypothesis that information to AI and AAF travels along independent processing streams despite widespread regional overlap of thalamic input sources. Double labeling is also sparse in both the corticocortical and commissural systems (~1%), confirming their independence. The segregation of frequency-specific channels within thalamic and cortical systems is consistent with a model of parallel processing in auditory cortex. The global convergence of cells outside the targeted frequency domain in AI and AAF could contribute to context-dependent processing and to intracortical plasticity and reorganization.**

**Keywords:** AAF, AI, branched axons, convergence, medial geniculate body, parallel processing, thalamocortical projections

## Introduction

Contemporary models of cortical function have often emphasized the contribution of either thalamic (Reid and Alonso, 1995; Miller *et al.*, 2001), corticocortical (Wallace *et al.*, 1991), or commissural (Imig and Brugge, 1978) connectivity. A thalamocentric or corticocentric perspective constrains understanding of how the convergence of these systems can influence an area. Numerical differences in thalamic and cortical input likely have important consequences for the extrinsic excitability of cortical neurons. Here we studied the individual and the collective contribution of these three systems to a common functional domain in two subdivisions of primary auditory cortex. In joint physiological-anatomical experiments, the tonotopic distribution of characteristic frequency (CF) was mapped in primary auditory cortex (AI) and the anterior auditory field (AAF) in cats. We next injected different, but equally sensitive, retrograde tracers at the same CF locus in AI and AAF. This permitted the direct comparison of the numerical strength of corticocortical, commissural, and thalamic convergence in the corresponding physiological locus in two adjoining areas in the same experiment. Between the two fields we found significant qualitative and quantitative differences in convergence with regard to these three projection systems.

A major issue is how the organization of CF is achieved in AI and AAF since each has a somewhat different tonotopic organization (Merzenich *et al.*, 1975; Knight, 1977). As far as is known there is a single continuous CF map in the ventral division of the medial geniculate body (MGB) (Aitkin and Webster, 1972; Imig and Morel, 1985), while at least five independent CF representations have been described in auditory cortex (Imig and Reale, 1980; Reale and Imig, 1980; Morel and Imig, 1987). How are these multiple representations achieved? If these several cortical CF maps arise from thalamic neurons with branched axons, as suggested by prior studies (Morel and Imig, 1987), then one might expect to find sparse corticocortical connections between similar frequency regions in tonotopic fields receiving many branched thalamic axons. In either case, the proportion of thalamic and cortical neurons projecting to the same CF in different areas has never been compared systematically.

A current model of auditory thalamocortical connectivity emphasizes point-to-point connectivity with little allowance for thalamic neurons with branched axons (Brandner and Redies, 1990). Such a paradigm is at odds with earlier studies which find a substantial proportion – up to 18% in certain projections – of double labeled thalamocortical cells (Morel and Imig, 1987). A strict point-to-point scheme is at variance with the pattern of thalamocortical projections to primary visual cortex (areas 17 and 18), which notes a significant proportion of thalamic Y cells that terminate in both areas via branched axons (Humphrey *et al.*, 1985b). Nevertheless, the predictions of the point-to-point model have never been tested in AAF using modern tracers.

A related issue is whether AI and AAF are one region with a double representation of frequency or two functional areas. Hierarchically, they appear to be equivalent (Rouiller *et al.*, 1991), though prior work concluded that the ventral division of the medial geniculate body had a minor projection to AAF (Morel and Imig, 1987). The physiological data available show both similarities (Eggermont, 1998) and differences between AI and AAF (Schreiner and Urbas, 1988; Valentine and Eggermont, 2001; Noreña and Eggermont, 2002). The present results, when viewed within the context of thalamic and cortical connectivity, suggest that parallel streams of spectral information reach AI and AAF and that the input from each of the extrinsic sources is largely independent. Understanding how auditory thalamic and cortical inputs reach the tonotopic subregions of auditory cortex is a first step in establishing

where any independent representations of frequency are achieved and how they are preserved at still higher levels. It also addresses the question of whether this parallel segregation of pathways is a general property of auditory forebrain organization that might be related to the two afferent streams observed within primate auditory cortex (Rauschecker *et al.*, 1997; Romanski *et al.*, 1999).

## Materials and Methods

### *Surgical Preparation*

Experiments were conducted on the right auditory cortex of four adult cats, three female and one male, following protocols approved by the Institutional Animal Care and Use Committee of the University of California at San Francisco and the National Institutes of Health guidelines. Animals were sedated with ketamine (22 mg/kg, i.m.) and acepromazine (0.11 mg/kg, i.m.) and anesthetized with sodium pentobarbital (15–30 mg/kg, i.v.) before tracheotomy and subsequent surgical procedures. The head was immobilized while leaving the ears unobstructed. The skull and tissues overlying AI and AAF were removed and the brain surface was covered with silicon oil.

After the cortical exposure was completed, the animals received a constant infusion of ketamine (2–10 mg/kg/h), diazepam (0.05–0.2 mg/kg/h) and lactated Ringer's solution (1–3 ml/kg/h), except for one case that was infused with sodium pentobarbitol and lactated Ringer's solution. The animals were hydrated continuously and the body temperature was maintained at ~37 C with a feedback-controlled waterpad. Electrocardiogram and respiration were monitored continuously.

### *Physiological Mapping*

During the first 24 h of recording, CFs were mapped in AI and AAF to identify isofrequency contours and the borders between fields. The CF was defined by the frequency at which a response was elicited by the lowest sound pressure level. The mapped area of AAF was constrained by the sulcal pattern and by unresponsiveness at the low-frequency pole. The dorsal and ventral borders of AI were identified based on decreased tonotopy, broader tuning and decreased or absent auditory responsiveness. Parylene-coated tungsten microelectrodes (0.5–2.5 MΩ) were used to record single- and multi-unit activity from the main thalamic recipient zone, layers IIIb and IV, at depths of 700–1100 m (Winer, 1984a).

Tone bursts (3 ms linear rise and fall; 50 ms total duration; 400–700 ms interstimulus interval) were generated by a microprocessor (TMS32010, 16-bit D–A converter at 120 kHz) and presented through a STAX-54 headphone tube (Sokolich, US Patent 4251686, 1981) inserted into the left external meatus. To map unit responses, 675 pseudorandom tone bursts were presented at different frequencies (range 3–5 octaves) and intensities (range 70 dB). From the responses, an excitatory frequency response area was generated to determine CF. Post-experiment physiological analysis used MATLAB (MathWorks, Natick, MA). Tonotopic maps were depicted with the Voronoi–Dirichlet tessellation (DELDIR, Statlib, Carnegie Mellon University, Pittsburgh, PA), where polygon borders are defined by the midpoints between adjacent recording sites (Kilgard and Merzenich, 1998).

### *Tracer Injection and Perfusion*

Following the initial physiological mapping, retrograde tracers, cholera toxin beta subunit (CTβ) or cholera toxin beta subunit conjugated with gold (CTβG; List Biological Laboratories, Campbell, CA), were injected into matching isofrequency loci in AI and AAF. Glass pipettes with a 20–30 m tip diameter and containing mineral oil were filled with tracer and lowered to 500, 1000 and 1500 m below the pia. At each depth, a nanoliter injector (World Precision Instruments, Sarasota, FL) deposited 55.2 nl of tracer at a rate of 4.6 nl/15 s. An interval between deposits allowed for tracer equilibration before pipette withdrawal.

After the deposits, the animal was maintained for 48–52 h to allow for tracer transport and further physiological recordings. Animals then received a lethal dose of sodium pentobarbital and were perfused transcardially with 0.01 M phosphate buffered saline (PBS) followed by 4% paraformaldehyde/0.01 M PBS. The brain was dissected and cryoprotected in 30% sucrose/4% paraformaldehyde/0.01 M PBS for 3 days.

### *Histology*

Transverse sections were cut on a freezing microtome at 60 m and a 1:6 series was processed for the tracers. To visualize CTβG labeling, sections were rinsed in 50% ethanol, washed in double distilled water, silver-intensified for 3 h (Kierkegaard and Perry Laboratories, Gaithersburg, MD), washed in 1% sodium thiosulfate, then washed in 0.01 M PBS.

For CTβ labeling, sections were blocked for 1 h in 5% normal rabbit serum/0.3% Triton X-100, incubated overnight in a 1:7500 dilution of goat anti-CTβ primary antibody (List Biological Laboratories, Campbell, CA) in 0.01 M PBS, then processed using a goat Vectastain avidin–biotin–peroxidase (ABC) kit (Vector Laboratories, Burlingame, CA) with diaminobenzidine (DAB) as the chromogen. Sections were mounted onto gelatin-coated slides, cleared and coverslipped.

### *Cytoarchitectonic Analysis*

Adjacent series of sections were stained for the determination of thalamic subdivisions and cortical areas with the Nissl stain and the SMI-32 antibody, which recognizes neurofilaments in pyramidal neurons (Campbell and Morrison, 1989) and defines AI. For SMI-32 immunostaining, sections were blocked for 1 h in 5% normal horse serum/0.3% Triton X-100, incubated overnight in a 1:2000 dilution of the SMI-32 antibody (Sternberger Monoclonal Inc., Baltimore, MD), then processing with a mouse Vectastain ABC kit (Vector Laboratories) and a heavy-metal intensified DAB chromogen (Adams, 1981). Sections were mounted, cleared and coverslipped.

### *Anatomical Analysis*

Retrogradely labeled cell bodies were charted with a microscope connected to a motorized stage, using an imaging system superimposed on the microscope field (Lucivid) and a computer equipped with the Neurolucida plotting and analysis software (MicroBrightField, Colchester, VT). The thalamic and cortical labeling was plotted using the Neurolucida at 200×. These plots were imported to the Canvas graphics software package (Deneba Software Inc., Miami, FL) and aligned with scanned 15× drawings made independently of the subdivisions from Nissl preparations. Plots of cortical sections were reconstructed using the three-dimensional solids module in the Neuroexplorer analysis software (MicroBrightField). The three-dimensional model was processed in Canvas and aligned with sulcal landmarks from photographs of the brain to reconstruct lateral, surface views of cortical labeling. Counts of labeled cell populations and other quantitative measures were then made with Neuroexplorer. Statistical analysis was performed using the Prism software package (GraphPad Software, San Diego, CA).

## Results

A defining feature of AI and AAF is their tonotopic organization. By limiting the study of their connectivity to a narrow frequency range, a more precise picture of the similarities and differences in their convergent projections can be achieved. Frequency mapping in AI and AAF revealed the predicted systematic representations of frequency; however, their organization was not identical (Fig. 1*A*,*C*). Single- and multiunit extracellular maps of AI and AAF from two representative hemispheres (Fig. 1*A*,*C*: polygons represent Voronoi–Dirichlet tessellations; see Materials and Methods) showed a frequency reversal at the AI–AAF border (Fig. 1*A*,*C*: dashed lines). In each hemisphere ~150 points were mapped at a uniform spatial resolution and the resulting distribution of frequencies was evaluated. The representation of mid-frequencies in AAF (green and yellow polygons in Fig. 1*A*,*C*) was smaller and more patchy than in AI, suggesting they are underrepresented and

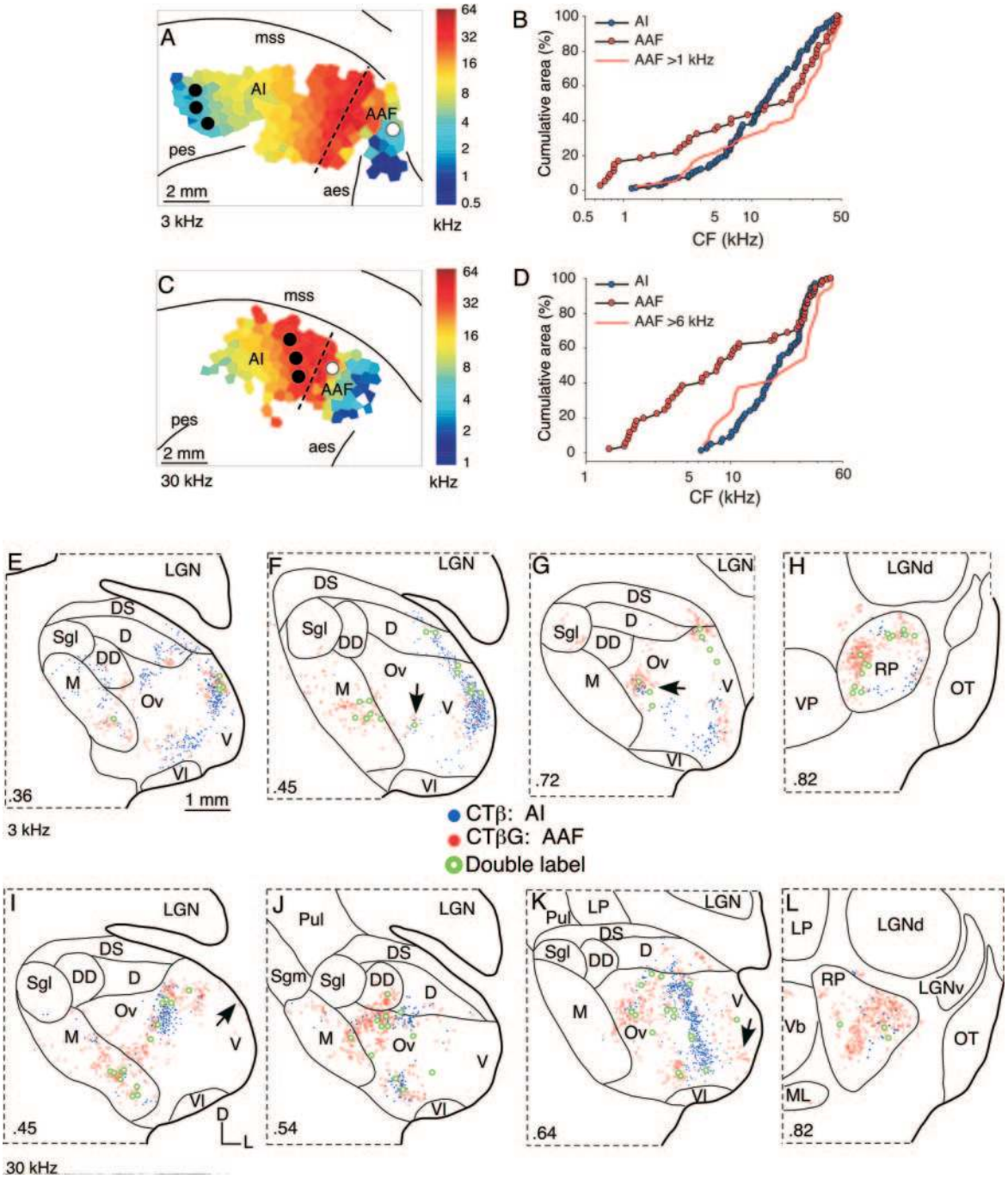


**Figure 1.** Distribution of characteristic frequencies (CFs) in AI and AAF and the ensuing patterns of thalamic retrograde labeling from two representative cases after tracer deposits at either low (3 kHz; *A*, *B*, *E–H*) or high (30 kHz; *C*, *D*, *I–L*) frequency loci. (*A*, *C*) Voronoi–Dirichlet tessellations illustrate the spatial distribution of CFs across AI and AAF. Circles indicate the location and size of the retrograde tracer injections. A dashed line approximates the AI/AAF border. (*B*, *D*) Quantitative measures of the CF distribution plotted against the cumulative area mapped (red and blue circles). To compare directly the cumulative CF distributions, the AAF distribution was replotted for a CF range matching that in AI (blue circles and red line). Unit penetrations spanning the border between AI and AAF, nine and ten cells in *B* and *D*, respectively, were included in both plots. Note the underrepresentation of middle-frequencies in AAF. (*E–L*) Plots of retrogradely labeled thalamic neurons after injections at either low *(E–H)* or high (*I–L*) frequency locations. The cells projecting to AI (blue dots) lie mainly in the ventral division (V) and are largely segregated from the cells projecting to AAF (red dots), which concentrate in the rostral pole (*L*: RP). The few neurons labeled in the suprageniculate nucleus (Sgl) were unique to this experiment. Double-labeled cells (green circles) are sparse (<3%). Other cells occupy heterotopic positions outside the frequency-matched locations (arrows). Decimals, the section position as a percentage of the total caudal–rostral length of the medial geniculate body. Abbreviations used in all figures: AAF, anterior auditory field; aes, anterior ectosylvian sulcus; AI, primary auditory cortex; AII, secondary auditory cortex; CF, characteristic frequency; Cg, cingulate gyrus; CTβ, cholera toxin beta subunit; CTβG, cholera toxin beta subunit, gold-conjugate; D, dorsal nucleus of the medial geniculate body, or dorsal; DD, deep dorsal nucleus of the medial geniculate body; DS, dorsal superficial nucleus of the medial geniculate body; EPD, posterior ectosylvian gyrus, dorsal part; EPI, posterior ectosylvian gyrus, intermediate part; EPV, posterior ectosylvian gyrus, ventral part; Ins, insular cortex; LGN, lateral geniculate nucleus; LGNd, dorsal lateral geniculate nucleus; LGNv, ventral lateral geniculate nucleus; LP, lateral posterior nucleus; M, medial division of the medial geniculate body, or medial; mss, middle suprasylvian sulcus; OT, optic tract; Ov, ovoid part of the medial geniculate body; P, posterior auditory cortex; pes, posterior ectosylvian sulcus; Pul, pulvinar; RP, rostral pole division of the medial geniculate body; SF, suprasylvian fringe cortex (dorsal auditory zone); Sgl, suprageniculate nucleus, lateral part; Sgm, suprageniculate nucleus, medial part; Te, temporal cortex; V, ventral division of the medial geniculate body, or ventral; Vb, ventrobasal complex; Ve, ventral auditory area; Vl, ventrolateral nucleus of the medial geniculate body; VP, ventral posterior auditory area; 35/36, parahippocampal areas 35 and 36.

discontinuous. To quantify this, the area of each polygon was computed and normalized to the mapped AI or AAF area from which we recorded. Cumulative plots were used to compare the CF representations in AI and AAF, with shallow slopes corresponding to smaller CF representations. In the AAF area plots (Fig. 1*B*,*D*: red circles), steps and subregions with shallow gradients occurred mainly in the 5–20 kHz mid-frequency region. The steps were not artifacts of systematic undersampling in certain subareas due to the presence of large blood vessels, but reflected inequalities in the areal assignment of frequency. By contrast, the AI area plot (Fig. 1*B*,*D*: blue circles) was smooth and homogeneous, suggesting nearly unbiased CF distribution for the entire mapped frequency range. Since the mapped CF ranges for AI and AAF differed due to the limited recording time, differences in cortical magnification factors, and sulcal patterns (Merzenich *et al.*, 1975; Reale and Imig, 1980), the distribution of cumulative areas was also compared within matched CF ranges (Fig. 1*B*,*D*: red line). Segments with shallow slopes in the mid-frequency range for AAF were maintained, suggesting that CF representation in AAF is smaller and less homogeneous than that in AI (Imaizumi *et al.*, 2003).

From the CF maps, tonotopically-matched subregions in AI and AAF were identified and injected with tracers. Two representative experiments, one with low- (3 kHz; Fig. 1*A*,*B*) and one with high-frequency (30 kHz; Fig. 1*C*,*D*) injections are shown; the other cases had comparable origins, topography, numbers of labeled neurons and patterns of retrograde labeling (Table 1). Since the CF representation is larger in AI due to an expanded magnification factor, three CTβ deposits were made along an AI isofrequency contour (Figs 1*A*,*C*: black dots; Fig. 3*A*) and one of CTβ conjugated to gold particles (CTβG) at a matching frequency in AAF (Fig. 1*A*,*C*: white dot; Fig. 3*B*). Each injection site was <1 mm in diameter, including diffusion, and did not enter the white matter (Fig. 3*A*,*B*). The position of the bulk of labeling in the thalamus and in the ipsilateral and contralateral cortex, was consistent and closely related to CF in all experiments.

### *Thalamic Projections*

Deposits in low frequency parts of AI labeled several clusters of cells in the MGB, mainly in the lateral part of the ventral division (Fig. 1*E–G*: V, blue dots), in accord with physiological studies (Aitkin and Webster, 1972). Neurons labeled by the low-frequency AAF CTβG deposit (Fig. 1*E–H*: red dots) also formed clusters that partially overlapped the clusters from the AI deposit. Circumscribed cell clusters were present in the medial and dorsal divisions. Other labeled cells showed a more diffuse spatial distribution in tonotopically inappropriate (heterotopic) positions. Such heterotopic labeling was present after low- (Fig. 1*F*,*G*: arrows) and high-frequency (Fig. 1*I*,*K*: arrows) deposits and reflected both CTβ and CTβG labeling. In the high-frequency deposits, the foci of CTβ and CTβG labeling lay ~1.5 mm apart, with the CTβG labeled cells dispersed across almost 5 mm in the mediolateral axis. Few neurons (1.6 ± 0.3%) were double labeled (Table 2; Fig. 1*E–L*: large green circles; Fig. 3*C*: 3) in any experiment, further attesting to the independence of these thalamocortical systems.

In the MGB, three of five main nuclei, including the ventral division, the rostral pole, which has also been designated as the lateral part of the posterior group (Morel and Imig, 1987), and the medial division, showed statistically significant differences ($P < 0.05$, two-tailed paired $t$-test, df = 3) in their projections to AI and AAF (Table 3; Fig. 4*A*: thalamus) when the proportion of labeled cells in each was compared. Projection strength comparisons from the dorsal division nuclei showed no significant difference between the two fields. This suggests different thalamic origins for information sent to spectrally congruent locations of these two cortical regions.

### *Corticocortical Projections*

Ipsilateral connections comprised ~70% of the total number of extrinsic cells projecting to both AI and AAF (Table 1). For the low-frequency injection, large parts of ipsilateral AI, including high- and low-frequency regions (Merzenich *et al.*, 1975), had CTβ-labeled cells (Fig. 2*A*). These intrinsic projections were generally restricted along a dorsal–ventral axis, consistent with similar best frequencies. Nearly all ipsilateral fields had many labeled neurons, with significant numbers in heterotopic territories outside tonotopic subregions (Imig and Reale, 1980) in every field. This included AI, where labeling far from the injected CF was evident (Fig. 2*A*: arrow). Indeed, while most of the AI projection arose topographically and from tonotopically appropriate loci, there were scattered neurons in all sectors except its rostral pole and extending to the borders of adjoining fields. The dorsal part of the posterior area (P) and

**Table 1**
Number of neurons and percentages of extrinsic convergent projections to AI and AAF

| Case | Frequency (kHz) | Total neurons[a] | | Extrinsic[b] | | Thalamus[c] | | Corticocortical[c] | | Commissural[c] | |
|---|---|---|---|---|---|---|---|---|---|---|---|
| | | AI | AAF | AI | AAF | AI | AAF | AI | AAF | AI | AAF |
| 1561 | 7 | 18 476 | 16 794 | 46.1 | 28.4 | 10.2 | 11.5 | 75.0 | 75.3 | 14.8 | 14.2 |
| 1568 | 30 | 21 816 | 54 677 | 40.8 | 52.2 | 10.6 | 7.0 | 75.6 | 85.7 | 13.8 | 7.3 |
| 1572 | 3 | 18 095 | 39 853 | 42.1 | 38.8 | 15.7 | 8.7 | 63.6 | 75.9 | 20.7 | 15.4 |
| 1599 | 20 | 11 274 | 31 191 | 33.7 | 35.7 | 25.7 | 16.7 | 56.9 | 69.5 | 17.4 | 13.8 |
| Mean | | 17 415 | 35 628 | 40.7 | 38.8 | 15.5 | 11.0 | 72.2 | 76.6 | 14.7 | 12.7 |
| SE | | 2211 | 7932 | 2.6 | 5.0 | 3.6 | 2.1 | 3.1 | 3.4 | 1.3 | 1.8 |

[a]Total number of intrinsic and extrinsic neurons.
[b]Percentage of the total number of neurons projecting from extrinsic sources.
[c]Percentage of extrinsic projections from thalamus, ipsilateral or commissural cortex, respectively.

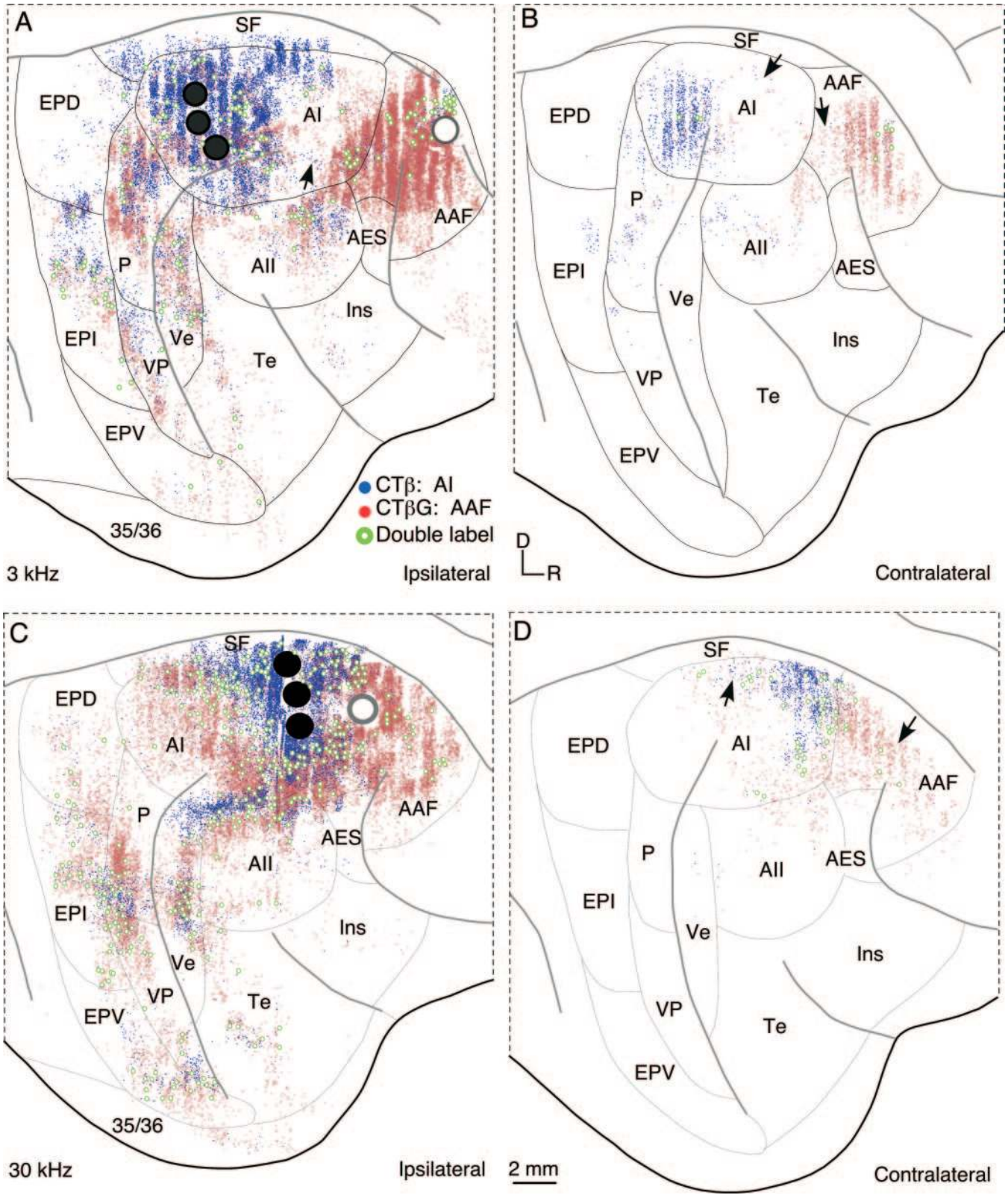


**Figure 2.** Lateral views of plots of retrogradely-labeled neurons projecting to AI (blue dots), AAF (red dots), or both (green circles) in the ipsilateral (*A*, *C*) and contralateral (*B*, *D*) cortex from the experiments shown in Figure 1. Large circles indicate injection sites. To facilitate comparison, the contralateral hemispheres match the ipsilateral orientation. (*A*, *C*) Both AI and AAF receive massive convergent topographic input from intrinsic, tonotopic (P, VP, Ve), and non-tonotopic (AII, Ins, Te, EP, SF) sources. Differential connections from the suprasylvian fringe (SF) and the cingulate (not shown) and parahippocampal (35/36) cortex distinguish the fields. The vertical aliasing of the labeled cells is an artifact from aligning the plotted sections; the labeling is actually continuous. The large number of intrinsic projection neurons in AI and AAF obscures many of the cross-projecting neurons in these fields. (*B*, *D*) Parallel commissural projections link AI and AAF with the contralateral homotopic area. In both hemispheres, few neurons project to both fields (<3%). In contrast, many more neurons (~15%) are in tonotopically inappropriate (heterotopic) locations (arrows).

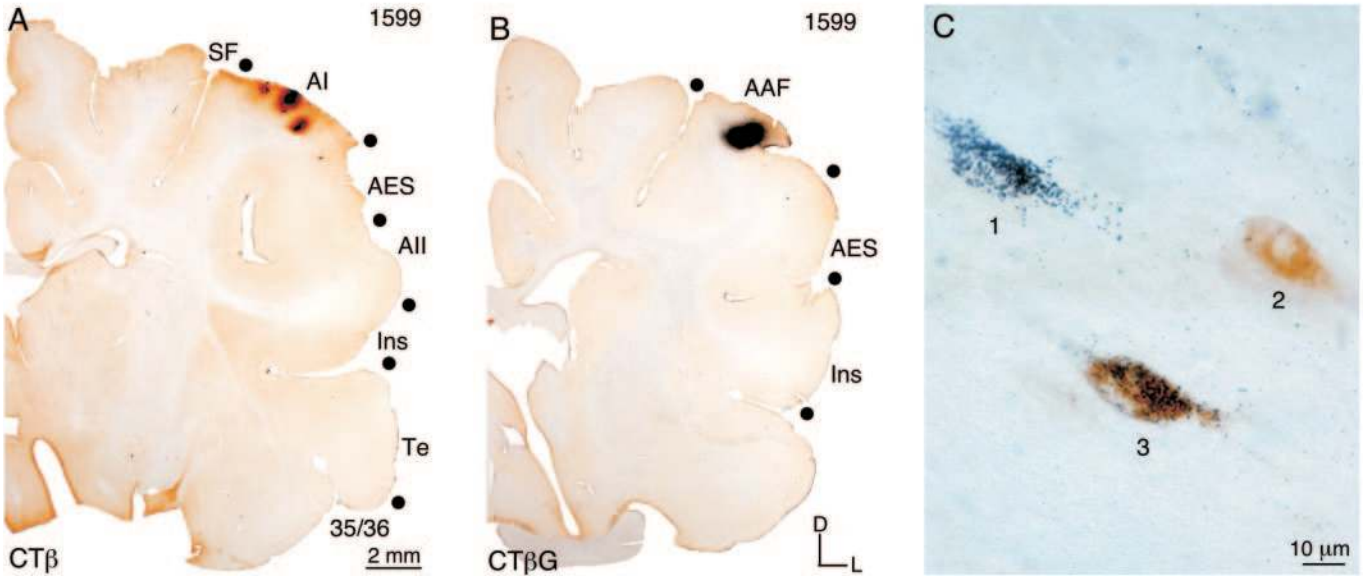


**Figure 3.** Representative deposit sites and ensuing thalamic retrograde labeling. (*A*) Tracer deposits in AI; the central deposit is near the center of its maximum size. (*B*) Corresponding deposit from the frequency-matched AAF site (upper right corner). (*C*) The three types of retrograde labeling were CTβ-gold alone (1), CTβ-gold alone (2) and double-labeling (3).

**Table 2**
Percentage of neurons projecting to both AI and AAF

| Case | Frequency (kHz) | Thalamus[a] | Corticocortical | Commissural |
|---|---|---|---|---|
| 1561 | 7 | 1.6 | 0.5 | 0.3 |
| 1568 | 30 | 2.5 | 2.2 | 1.7 |
| 1572 | 3 | 1.2 | 0.7 | 0.1 |
| 1599 | 20 | 1.1 | 1.0 | 0.7 |
| Mean ± SE | | 1.6 ± 0.3 | 1.1 ± 0.4 | 0.7 ± 0.4 |

[a]Percentage.

**Table 3**
Percentage of thalamic projections by origin to AAF and AI

| | Tonotopic | | Broadly tuned | | |
|---|---|---|---|---|---|
| Area | V[a] | RP | D[b] | SgI | M |
| AAF | 40.5 ± 7.2* | 34.2 ± 2.5* | 12.3 ± 4.2 | 0.4 ± 0.3 | 12.6 ± 1.3* |
| AI | 77.9 ± 15.8 | 4.7 ± 0.7 | 11.2 ± 2.8 | 1.0 ± 0.6 | 5.2 ± 0.5 |

[a]Mean ± SE.
[b]Includes the dorsal (D), deep dorsal (DD), and dorsal superficial (DS) nuclei.
*Statistically significant, $P < 0.05$, df = 3, two-tailed paired *t*-test.

ventral part of the ventral posterior area (VP), both of which are tonotopic, each had many CTβ-positive cells (Fig. 2*A*). Lighter projections, which sometimes were sharply circumscribed (Fig. 2*A*), arose in non-tonotopic areas such as the dorsal, intermediate and ventral parts of the posterior ectosylvian cortex (EPD, EPI, EPV), from the second auditory area (AII) and the insular (Ins) and temporal (Te) fields, and this input was segregated topographically in each. The CTβG deposit labeled low frequency (rostral) AAF sectors and mid-frequency AI regions heavily and topographically in the ipsilateral hemisphere (Fig. 2*A*). Most corticocortical labeling had a restricted spatial distribution in every field, even in those without obvious tonotopic organization, such as AII (Schreiner and Cynader, 1984; Lee and Winer, 2003). The CTβ labeling did not extend as far caudally as in the first experiment except at the dorsal and ventral parts of AI. Likewise, the CTβG labeling filled most of AAF and extensive mid-frequency AI territories.

Nearly all of AAF was labeled by the deposit in it, including heterotopic regions far from the injected CF region, contrasting with the more confined intrinsic projections of AI. In the same experiment, rostral and central AI clusters of CTβG labeling were interspersed with islands of CTβ-positive cells; this arrangement was seen in areas P, Ve, VP and EPI in both low- (Fig. 2*A*) and high-frequency (Fig. 2*C*) experiments. Areas 35 and 36 (the parahippocampal gyrus) were labeled differentially by deposits in high- and low-frequency AAF (cf. Fig. 4*A*: ipsilateral cortex).

Few double labeled neurons were found (Fig. 2*A*,*C*: open circles), with more in the high-frequency experiment (2.2 versus 0.7%) where the deposit sites were closest (~1.5 mm apart; Table 2). The laminar projections interconnecting AI and AAF originated from layers II, III, V and VI, whereas the input from the other areas mainly arose in layers V and VI (data not shown).

The numerical weight of projections to each field differed significantly, as shown when the areas were arranged hierarchically on the basis of the relative numerical strength of their projection (Fig. 4*B*). Areas with projections that did not differ significantly (ANOVA) are assigned to the same hierarchical level. The resulting order differs for the two target fields, suggesting a functional distinction between them. The strongest projections originated from the intrinsic projections within an area (Fig. 4*B*: rank 5) followed by the extrinsic projections between the two areas (Fig. 4*B*: rank 4). The other tonotopic areas (P, VP, Ve) and, surprisingly, AII provided the next largest set of projections (Fig. 4*B*: rank 3), while projections from posterior ectosylvian (EPD, EPI, EPV) and limbic/

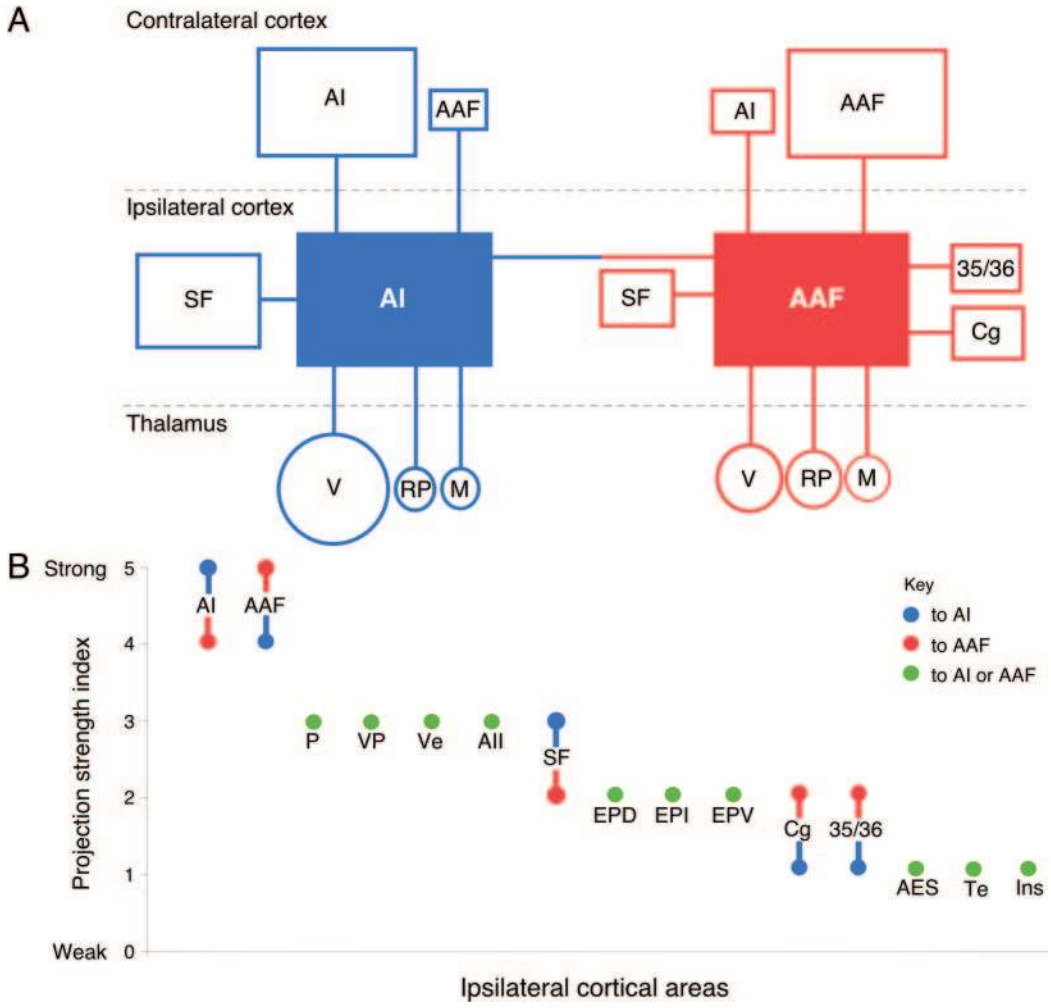


**Figure 4.** (*A*) Graphic summary of statistically significant differences in the projections to AI (blue) and AAF (red) from the thalamus and ipsilateral and contralateral cortex. The area of each contour is proportional to the relative strength of the input from each source. AI receives its major thalamic input from the ventral division (V) and substantial cortical projections from the suprasylvian fringe (SF) and the contralateral AI. By comparison, AAF has larger input from the rostral pole (RP) and medial division (M) of the medial geniculate body and the contralateral AAF, plus unique projections from the cingulate (Cg) and parahippocampal areas (35/36) that distinguish it from AI ($P < 0.05$, df = 3, two-tailed, paired *t*-test). (*B*) Hierarchical arrangement of corticocortical projections for AI and AAF. The projections to the two fields were ordered according to their proportion of the total number of projecting neurons. Levels ranged from weak to strong: (0) 0%, (1) 0.01–1%, (2) 1–5%, (3) 5–10%, (4) 10–15% of the total extrinsic projection (~40% of total combined input); level (5) represents the intrinsic projection within an area (~60% of total combined input). Fields with statistically indistinguishable projection sizes (ANOVA, $P > 0.05$) were assigned to the same hierarchical level.

association areas (AES, Te, Ins) formed two groups, respectively, of weaker connections (Fig. 4*B*: ranks 2 and 1). Three other regions, the suprasylvian fringe cortex (SF), parahippocampal areas (35/36) and the anterior cingulate cortex (Cg), differed significantly in their relative input, confirming further differences between AI and AAF (Fig. 4*A*,*B*).

### *Commissural Projections*

Commissural projections comprised ~15% of the input to AI and AAF (Fig. 2*B*,*D*), far less than the corticocortical (Fig. 2*A*,*C*) projection. The heaviest foci of CTβ and CTβG labeling were in regions matching spatially the contralateral deposit site, though many heterotopic cells were far beyond the <1 mm diameter of the deposit, particularly in the high frequency sectors of AI and AAF (Fig. 2*B*: arrows). The labeling elsewhere was lighter but still clustered spatially. Thus, AII contained caudal foci of CTβ and rostral CTβG labeling, with little overlap. In the high-frequency case commissural labeling was again lighter and concentrated in mirror image to the deposit site, except for the low frequency sector of AAF (Knight, 1977) and in central AI (Fig. 2*D*: arrows), where it was heterotopic and unexpectedly robust. The remaining projections were far lighter and always involved the same fields as the ipsilateral labeling. Once again, there was connectional topography even among non-tonotopic fields: in the ipsilateral AII, the projection shifted from rostrodorsal, in the 3 kHz case, to caudoventral, in the 30 kHz case. The two commissural areas showed significant differences in their AI/AAF projections (Fig. 2*B*,*D*: commissural; Fig. 4*A*: contralateral cortex). The principal homotopic labeling in both areas arose from neurons in layers III and V, but differed in their relative contributions [layer III/V ratio: AI (~70/30%), AAF (~50/50%); data not shown].

Double labeling was again sparse (0.7 ± 0.4%) and more prominent in the high- than the low frequency (1.7 versus 0.1%) cases, where the deposits were much nearer (Table 2)

and where the cortical frequency representation is more compressed than that at lower CFs (Merzenich *et al.*, 1975).

## Discussion

Physiological mapping in conjunction with anatomical tracing of thalamic, corticocortical and commissural projections reveals independent projections to areas AI and AAF, with few neurons in any source of extrinsic input terminating in both areas. This finding is interpreted within the context of parallel processing for spectral information.

### *Methodological Issues*

Earlier conclusions regarding local and ipsilateral connections for AI and AAF were based on much larger deposits and used less sensitive tracers or methods that could injure axons inadvertently (Diamond *et al.*, 1968; Kawamura, 1973) or tracer deposits so small that they might fail to saturate fully a pia-to-white-matter column (Matsubara and Phillips, 1988). We used highly and equally sensitive tracers (Ruigrok *et al.*, 1995) with little capacity for diffusion (Llewellyn-Smith *et al.*, 1990) and whose limits could be estimated accurately in these mapped hemispheres. We find that the corticocortical system has wider areal inputs and larger within-area projections than are predicted by point-to-point homotypic models (Brandner and Redies, 1990) of thalamic projections (cf. Fig. 5*C*). In none of the 16 deposit sites in four hemispheres was there significant involvement of the white matter. Thus, any contribution from severed fibers was deemed to be negligible (Chen and Aston-Jones, 1995).

One interpretive caveat to the present results is that we have not performed experiments in which the two tracers were mixed and injected at a single locus, which ought to label nearly all cells in the center of the heaviest concentrations. It is, therefore, possible that our estimates of double labeling are unduly low.

### *Validity of Heterotopic Projections*

The thalamic retrograde labeling arose from much larger medial geniculate body territories than appear to be devoted to the CF representation injected in prior mapping studies (Aitkin and Webster, 1972; Imig and Morel, 1984). Thus, the 3 kHz deposit arose from thalamic cells separated in the medio-lateral dimension by up to 5 mm and by ~3 mm in the 30 kHz experiment, respectively. Thalamic labeling in other experiments had an analagous distribution (data not shown). We estimate that our deposits were restricted to ~10% of the surface area of AI and AAF and are thus centered within targeted isofrequency domains even as they spread slightly toward higher and lower adjoining frequencies. This would seem to preclude the unintended involvement of adjoining isofrequency regions, as does the breadth of the thalamic origins. Perhaps the less complete and more variable CF gradient in AAF contributes to the appearance of a wider distribution of the input sources than in AI. At least parts of the thalamic (Morel *et al.*, 1987) and cortical (Schreiner and Sutter, 1992) isofrequency representations must include heterotopic cells outside the CF domain as demonstrated in fine-grain mapping studies where the responses in single, near-vertical electrode penetrations often span ~3 octaves (Imig and Morel, 1985; Morel *et al.*, 1987). The present results suggest that such variability of topographic representation is a natural component of the isofrequency domain. The same principle of heterotopic origins applies to the ipsilateral, corticocortical and commissural projections.

### *Comparison with Other Studies of Thalamocortical Projections*

The massive labeling (several thousand cells from even one spatially confined deposit) suggests that the magnitude of thalamic and cortical projections in older studies that used less sensitive methods (Winer *et al.*, 1977; Niimi and Matsuoka, 1979; Andersen *et al.*, 1980) may have been underestimated.

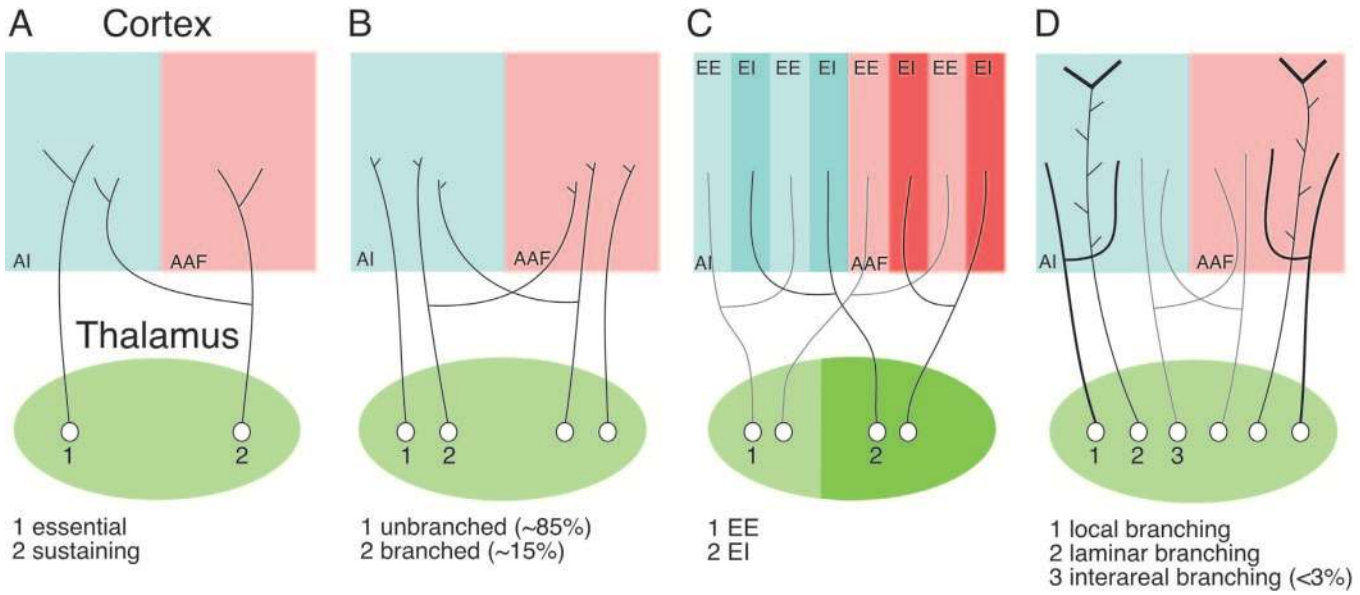


**Figure 5.** Schematic models of the auditory thalamocortical projection. (*A*) Essential and sustaining projections proposed by Rose and Woolsey (1958) suggested the existence of branched projections across areas. (*B*) While unbranched projections within an area predominate, interareal branching was believed to provide substantial input (~15%) (Imig and Morel, 1984). (*C*) Studies of thalamic projections to binaural subdomains indicate modular specificity of intraareal branching (Middlebrooks and Zook, 1983; Brandner and Redies, 1990). (*D*) Widespread laminar distribution of thalamic input (Huang and Winer, 2000), coupled with the present findings of sparse interareal divergence (present results), suggest that parallel streams originate from the thalamus and branch specifically within an area to support modular computations. Differences in the thickness of lines represents axons of different caliber. A similar model has been proposed in the rabbit auditory thalamocortical pathway (Velenovsky *et al.*, 2003).

While many of the projection patterns noted here have been seen in earlier work, several others have not been previously documented and the robust labeling implies a richness of connectivity not evident with other methods.

We found a small projection from the dorsal division to AI and AAF that constituted <10% of the thalamic projection. It is difficult to compare the present study to prior work (Andersen *et al.*, 1980) since the latter study used tracers which labeled only a fraction of the thalamocortical connections seen here. Moreover, since thalamic boundaries were not included (e.g. their Figures 8 and 10), any direct comparison is constrained. In contrast, we found only modest input from the dorsal division to both AI and AAF in all but one experiment. Likewise, another study that used horseradish peroxidase, wheat germ agglutinin, or [$^3$H]bovine serum albumin (Morel and Imig, 1987) as retrograde tracers, found a different pattern of thalamocortical projections than we did. For example, they saw little labeling in the ventral division with horseradish peroxidase alone and a concentration of cells in the rostral pole of the medial geniculate body (their Fig. 12) after 4 tracer deposits in AAF. Our single, much smaller AAF deposit (Fig. 1*A*,*C*) produced the same pattern of labeling in the rostral pole of the medial geniculate body and labeled far more cells in the ventral division than would have been expected by the previous studies. We attribute this to the superior sensitivity of the newer tracers. Beside the unexpected ventral division projection to AAF, the rostral pole had a larger than predicted input to AI (Table 3: rostral pole). This suggests a closer alignment of AI and AAF in their thalamic, but not in their extra-auditory, cortical input (Fig. 4*A*).

### *Comparison with Prior Work on Corticocortical Projections*

Previous studies showed more restricted corticocortical origins (Matsubara and Phillips, 1988; Wallace *et al.*, 1991) than those from our deposits. We found ipsilateral labeling within AI and AAF up to 3 mm from the deposits; these heterotopic projections are far from the deposit sites and well beyond the boundaries predicted by their CF organization (Fig. 2*A*,*C*). The breadth of these intrinsic connections was larger in AAF, suggesting greater convergence of local input to a frequency domain than in AI.

Other corticocortical retrograde labeling had even more remote areal origins and was robust. The laminar sources of these projections to both fields from outside areas involve mainly the deep cortical layers, which are associated with feedback connections (Felleman and Van Essen, 1991). This is consistent with an early position for both AI and AAF in hierarchical models of auditory cortical processing (Rouiller *et al.*, 1991).

Virtually all auditory areas, primary and non-primary, converge upon AI. There is also input unique to AI from non-primary areas related to duration processing (suprasylvian fringe; He *et al.*, 1997) and whose role in AI function is unknown. This implies that AI and AAF cells receive massive convergent input complementary to their divergent outputs (Imig and Reale, 1980). The corticocortical connections of AAF also set it apart from AI. Thus, input to AAF arises from unexpected sources as remote as the parahippocampal and cingulate gyri, regions associated with auditory attention (anterior cingulate gyrus; Benedict *et al.*, 2002; Sevostianov *et al.*, 2002) and learning and memory (parahippocampal gyrus; Burwell, 2002). AI and AAF thus have shared input from tonotopic auditory cortical areas, while a different pattern of limbic and peri-auditory input sets AAF apart (Fig. 4*A*: ipsilateral cortex).

The spatial breadth of these connections might explain why inactivating one tonotopic field could have so little effect on another (Kitzes and Hollrigel, 1996), why lesions involving many auditory areas (Neff *et al.*, 1975) are required to produce global effects on behavior, and they could underlie other functional distinctions between AI and AAF (Ehret, 1997).

### *Branched Axons are Rare in the Auditory Forebrain*

The percentage of double labeled neurons in the present study is much smaller than that seen using other methods (Morel and Imig, 1987), despite the fact that our experimental design and the sensitivity of the tracers ought to have maximized their number and detection. This is consistent with the idea of independent connectional systems and this principle was conserved in all three types of connections. This implies a fundamental difference between the auditory forebrain and the brainstem, where axons subdivide profusely to innervate many different targets (Irvine, 1986). Such a pattern would seem to set the auditory forebrain apart from the visual cortex (Bullier *et al.*, 1984).

### *Functional Implications*

We find differences in the CF representations and its distributions in AI and AAF that support the notion of separate functional roles. Previous work also noted that AAF neurons have slightly shorter latencies, lower thresholds, broader tuning curves and higher spontaneous rates of discharge (Eggermont, 1998; Valentine and Eggermont, 2001; Noreña and Eggermont, 2002; Imaizumi *et al.*, 2003) than AI neurons. Prospective differences between AI and AAF pertain to responses to dynamic stimuli, such as frequency or amplitude modulations and vocalizations, many aspects of which either remain to be studied or are inconclusive (Schreiner and Urbas, 1988; Tian and Rauschecker, 1994; Eggermont, 1999). There are also functional parallels with tonal receptive field properties in both areas that are broadly distributed and largely overlapping. The differential homogeneity in AI and AAF frequency gradients (Fig. 1*B*,*D*) could either reflect unique inputs from thalamic (Middlebrooks *et al.*, 1980) and/or extrathalamic sources (Fig. 4*A*: AAF) or it might embody intrinsic cortical mechanisms for differential task- or context-dependent organizations and representational modulations (Weinberger, 1998; Kilgard and Merzenich, 2002).

The parallel nature of processing in AI and AAF is also supported by findings from cross-correlation analysis (Eggermont, 2000) that showed higher peak correlation coefficients for neurons from within AI, compared to correlations between the two fields. The very modest contribution from branching axons to the two fields may account for this difference in intra- versus inter-areal synchrony.

There are many instances of functional modularity in AI, such as binaural bands (Imig and Adrián, 1977) and spectral integration modules (Schreiner *et al.*, 2000). We find that such modularity of receptive field parameters, such as threshold, $Q_{10}$, $Q_{40}$ and latency, is less prominent in AAF, extending the functional distinctions between fields (Imaizumi *et al.*, 2003).

A functional difference attributed to subcortical processing is the spatial segregation of thalamic binaural input to AI (Middlebrooks and Zook, 1983; Velenovsky *et al.*, 2003) and

analogous commissural segregation (Imig and Adrián, 1977). There is no similar evidence available for AAF. This contrasts with subdivisions in primary visual (areas 17 and 18) and primary somatosensory (areas 3a and 3b) cortex where dominant inputs can be traced to segregated subcortical streams, e.g. visual X and Y cells (Humphrey *et al.*, 1985a), or module-specific segregation of receptor populations, e.g. somatosensory cutaneous and musculoskeletal receptors (Jones and Porter, 1980), that are presumably established in the periphery. Despite the many parallels between the auditory and visual systems, emergent global distinctions in the principles organizing thalamic (Huang and Winer, 2000; Smith and Populin, 2001), corticocortical (Read *et al.*, 2001) and commissural pathways (present results), as well as in neuronal morphology (Winer, 1984b; Smith and Populin, 2001), suggest modality-specific principles of organization.

### *Models of Thalamocortical Connectivity*

These results further refine and constrain the models of connectivity in the thalamocortical auditory system. From a historical perspective, it is possible to identify at least four models of thalamic input (Fig. 5). Single neurons were early proposed to have either an essential projection that terminated in one area and degenerated after large lesions of this area, while sustaining projections were preserved by collaterals to other, intact areas (Fig. 5*A*) (Rose and Woolsey, 1958). Experiments using a dual retrograde tracing strategy with sensitive tracers suggested that this interareal branching contributed a substantial fraction (~15%) of the thalamocortical input (Fig. 5*B*) (Morel and Imig, 1987). Subsequent work on divergence led to the idea that aurally specific thalamic neurons project to similar functional domains within an area (Fig. 5*C*) (Middlebrooks and Zook, 1983; Brandner and Redies, 1990; Velenovsky *et al.*, 2003). Analyses of the laminar distribution of the thalamic input has also demonstrated a network of input across several (and sometimes all) cortical layers (Fig. 5*D*) and finds that small deposits of anterograde tracers in the thalamus label highly divergent cortical terminal zones (Huang and Winer, 2000). The present findings suggest that interareal branching is sparse and, therefore, likely contributes little to the global distribution of information across fields (Fig. 5*D*). Rather, parallel systems of thalamocortical input terminate in each area, where they branch locally and across layers to support functional modularity and subsequent computations. It remains for future work to elaborate plausible models of commissural and ipsilateral corticocortical connectivity as part of a larger paradigm for understanding the ordinal flow of information through auditory cortex.

## Notes

We thank David Fitzpatrick and Edwin Rubel for advice, David Larue and Tania Bettis for histological assistance and Andrew Tan, Benedicte Philibert and Poppy Crum for their participation in the physiological recordings. These studies were supported by National Institutes of Health grants R01 DC2260-07 (C.E.S.) and R01 DC2319-24 (J.A.W.).

Address correspondence to Charles C. Lee, Department of Molecular and Cell Biology, Division of Neurobiology, Room 285 LSA, University of California at Berkeley, Berkeley, CA 94720-3200, USA. Email: chazwell@uclink4.berkeley.edu.

## References

Adams JC (1981) Heavy metal intensification of DAB-based HRP reaction product. J Histochem Cytochem 29:775.

Aitkin LM, Webster WR (1972) Medial geniculate body of the cat: organization and responses to tonal stimuli of neurons in ventral division. J Neurophysiol 35:365–380.

Andersen RA, Knight PL, Merzenich MM (1980) The thalamocortical and corticothalamic connections of AI, AII, and the anterior auditory field (AAF) in the cat: evidence for two largely segregated systems of connections. J Comp Neurol 194:663–701.

Benedict RHB, Shucard DW, Santa Maria MP, Shucard JL, Abara JP, Coad ML, Wack D, Sawusch J, Lockwood A (2002) Covert auditory attention generates activation in the rostral/dorsal anterior cingulate cortex. J Cogn Neurosci 14:637–645.

Brandner S, Redies H (1990) The projection of the medial geniculate body to field AI: organization in the isofrequency dimension. J Neurosci 10:50–61.

Bullier J, Kennedy H, Salinger W (1984) Bifurcation of subcortical afferents to visual areas 17, 18, and 19 in the cat cortex. J Comp Neurol 228:308–328.

Burwell RD (2002) The parahippocampal region: corticocortical connectivity. Ann N Y Acad Sci 911:25–42.

Campbell MJ, Morrison JH (1989) Monoclonal antibody to neurofilament protein (SMI-32) labels a subpopulation of pyramidal neurons in the human and monkey neocortex. J Comp Neurol 282:191–205.

Chen S, Aston-Jones G (1995) Evidence that cholera toxin B subunit (CTb) can be avidly taken up and transported by fibers of passage. Brain Res 674:107–111.

Diamond IT, Jones EG, Powell TPS (1968) The association connections of the auditory cortex of the cat. Brain Res 11:560–579.

Eggermont JJ (1998) Representation of spectral and temporal sound features in three cortical fields of the cat. Similarities outweigh differences. J Neurophysiol 80:2743–2764.

Eggermont JJ (1999) Neural correlates of gap detection in three auditory cortical fields in the cat. J Neurophysiol 81:2570–2581.

Eggermont JJ (2000) Sound-induced synchronization of neural activity between and within three auditory cortical areas. J Neurophysiol 83:2708–2722.

Ehret G (1997) The auditory cortex. J Comp Physiol A 181:547–557.

Felleman, DJ and Van Essen, DC (1991) Distributed hierarchical processing in the primate cerebral cortex. Cereb Cortex 1:1–47.

He J, Hashikawa T, Ojima H, Kinouchi Y (1997) Temporal integration and duration tuning in the dorsal zone of cat auditory cortex. J Neurosci 17:2615–2625.

Huang CL, Winer JA (2000) Auditory thalamocortical projections in the cat: laminar and areal patterns of input. J Comp Neurol 427:302–331.

Humphrey AL, Sur M, Uhlrich DJ, Sherman SM (1985a) Projection patterns of individual X- and Y-cell axons from the lateral geniculate nucleus to cortical area 17 in the cat. J Comp Neurol 233:159–189.

Humphrey AL, Sur M, Uhlrich DJ, Sherman SM (1985b) Termination patterns of individual X- and Y-cell axons in the visual cortex of the cat: projections to area 18, to the 17/18 border region, and to both areas 17 and 18. J Comp Neurol 233:190–212.

Imaizumi K, Priebe NJ, Crum PAC, Bedenbaugh PH, Cheung SW, Schreiner CE (2003) Modular functional organization in cat anterior auditory field. Proc Soc Neurosci 29:488.6.

Imig TJ, Adrián HO (1977) Binaural columns in the primary auditory field (A1) of cat auditory cortex. Brain Res 138:241–257.

Imig TJ, Brugge JF (1978) Sources and terminations of callosal axons related to binaural and frequency maps in primary auditory cortex of the cat. J Comp Neurol 182:637–660.

Imig TJ, Morel A (1984) Topographic and cytoarchitectonic organization of thalamic neurons related to their targets in low-, middle-, and high-frequency representations in cat auditory cortex. J Comp Neurol 227:511–539.

Imig TJ, Morel A (1985) Tonotopic organization in ventral nucleus of medial geniculate body in the cat. J Neurophysiol 53:309–340.

Imig TJ, Reale RA (1980) Patterns of cortico-cortical connections related to tonotopic maps in cat auditory cortex. J Comp Neurol 192:293–332.

Irvine DRF (1986) The auditory brainstem. A review of the structure and function of auditory brainstem processing mechanisms. In: Progress in sensory physiology (Autrum H, Ottoson D, Perl ER, Schmidt RF, Shimazu H, Willis WD, eds), pp. 1–279. Berlin: Springer Verlag.

Jones EG, Porter R (1980) What is area 3a? Brain Res Brain Res Rev 2:1–43.

Kawamura K (1973) Corticocortical fiber connections of the cat cerebrum. I. The temporal region. Brain Res 51:1–21.

Kilgard MP, Merzenich MM (1998) Cortical map reorganization enabled by nucleus basalis activity. Science 279:1714–1718.

Kilgard MP, Merzenich MM (2002) Order-sensitive plasticity in adult primary auditory cortex. Proc Natl Acad Sci USA 99:3205–3209.

Kitzes LM, Hollrigel GS (1996) Response properties of units in the posterior auditory field deprived of input from the ipsilateral primary auditory cortex. Hearing Res 100:120–130.

Knight PL (1977) Representation of the cochlea within the anterior auditory field (AAF) of the cat. Brain Res 130:447–467.

Lee CC, Winer JA (2003) Topographic projections in cat auditory cortex. Proc Soc Neurosci 29:592.15.

Llewellyn-Smith IJ, Minson JB, Wright AP, Hodgson AJ (1990) Cholera toxin B-gold, a retrograde tracer that can be used in light and electron microscopic immunocytochemical studies. J Comp Neurol 294:179–191.

Matsubara JA, Phillips DP (1988) Intracortical connections and their physiological correlates in the primary auditory cortex (AI) of the cat. J Comp Neurol 268:38–48.

Merzenich MM, Knight PL, Roth GL (1975) Representation of cochlea within primary auditory cortex in the cat. J Neurophysiol 38:231–249.

Middlebrooks JC, Dykes RW, Merzenich MM (1980) Binaural response-specific bands in primary auditory cortex (AI) of the cat: topographic organization orthogonal to isofrequency contours. Brain Res 181:31–48.

Middlebrooks JC, Zook JM (1983) Intrinsic organization of the cat's medial geniculate body identified by projections to binaural response-specific bands in the primary auditory cortex. J Neurosci 3:203–225.

Miller LM, Escabí MA, Read HL, Schreiner CE (2001) Functional convergence of response properties in the auditory thalamocortical system. Neuron 32:151–160.

Morel A, Imig TJ (1987) Thalamic projections to fields A, AI, P, and VP in the cat auditory cortex. J Comp Neurol 265:119–144.

Morel A, Rouiller E, de Ribaupierre Y, de Ribaupierre F (1987) Tonotopic organization in the medial geniculate body (MGB) of lightly anesthetized cats. Exp Brain Res 69:24–42.

Neff WD, Diamond IT, Casseday JH (1975) Behavioral studies of auditory discrimination: central nervous system. In: Handbook of sensory physiology. Vol. V, part 2, auditory system, anatomy, physiology (ear) (Keidel WD, Neff WD, eds), pp. 307–400. Berlin: Springer Verlag.

Niimi K, Matsuoka H (1979) Thalamocortical organization of the auditory system in the cat studied by retrograde axonal transport of horseradish peroxidase. Adv Anat Embryol Cell Biol 57:1–56.

Noreña A, Eggermont JJ (2002) Comparison between local field potentials and unit cluster activity in primary auditory cortex and anterior auditory field in the cat. Hearing Res 166:202–213.

Rauschecker JP, Tian B, Pons T, Mishkin M (1997) Serial and parallel processing in rhesus monkey auditory cortex. J Comp Neurol 382:89–103.

Read HL, Winer JA, Schreiner CE (2001) Modular organization of intrinsic connections associated with spectral tuning in cat auditory cortex. Proc Natl Acad Sci USA 98:8042–8047.

Reale RA, Imig TJ (1980) Tonotopic organization in auditory cortex of the cat. J Comp Neurol 182:265–291.

Reid RC, Alonso JM (1995) Specificity of monosynaptic connections from thalamus to visual cortex. Nature 378:281–284.

Romanski LM, Tian B, Fritz J, Mishkin M, Goldman-Rakic PS, Rauschecker JP (1999) Dual streams of auditory afferents target multiple domains in the primate prefrontal cortex. Nat Neurosci 2:1131–1136.

Rose JE, Woolsey CN (1958) Cortical connections and functional organization of thalamic auditory system of cat. In: Biological and biochemical bases of behavior (Harlow HF, Woolsey CN, eds), pp. 127–150. Madison, WI: University of Wisconsin Press.

Rouiller EM, Simm GM, Villa AEP, de Ribaupierre Y, de Ribaupierre F (1991) Auditory corticocortical interconnections in the cat: evidence for parallel and hierarchical arrangement of the auditory cortical areas. Exp Brain Res 86:483–505.

Ruigrok TJH, Teune TM, van der Burg J, Sabel-Goedknegt H (1995) A retrograde double-labeling technique for light microscopy. A combination of axonal transport of cholera toxin B-unit and a gold-lectin conjugate. J Neurosci Meth 61:127–138.

Schreiner CE, Cynader MS (1984) Basic functional organization of second auditory cortical field (AII) of the cat. J Neurophysiol 51:1284–1305.

Schreiner CE, Sutter ML (1992) Topography of excitatory bandwidth in cat primary auditory cortex: single-neuron versus multiple-neuron recordings. J Neurophysiol 68:1487–1502.

Schreiner CE, Urbas JV (1988) Representation of amplitude modulation in the auditory cortex of the cat. II. Comparison between cortical fields. Hearing Res 32:49–64.

Schreiner CE, Read HL, Sutter ML (2000) Modular organization of frequency integration in primary auditory cortex. Annu Rev Neurosci 23:501–529.

Sevostianov A, Fromm S, Nechaev V, Horwitz B, Braun A (2002) Effect of attention on central auditory processing: an fMRI study. Int J Neurosci 112:587–606.

Smith PH, Populin LC (2001) Fundamental differences between the thalamocortical recipient layers of the cat auditory and visual cortices. J Comp Neurol 436:508–519.

Tian B, Rauschecker JP (1994) Processing of frequency-modulated sounds in the cat's anterior auditory field. J Neurophysiol 71:1959–1975.

Valentine PA, Eggermont JJ (2001) Spontaneous burst-firing in three auditory cortical fields: its relation to local field potentials and its effect on inter-area cross-correlations. Hearing Res 154:146–157.

Velenovsky DS, Cetas JS, Price RO, Sinex DG, McMullen NT (2003) Functional subregions in primary auditory cortex defined by thalamocortical terminal arbors: an electrophysiological and anterograde labeling study. J Neurosci 23:308–316.

Wallace MN, Kitzes LM, Jones EG (1991) Intrinsic inter- and intralaminar connections and their relationship to the tonotopic map in cat primary auditory cortex. Exp Brain Res 86:527–544.

Weinberger NM (1998) Physiological memory in primary auditory cortex: characteristics and mechanisms. Neurobiol Learn Mem 70:226–251.

Winer JA (1984a) Anatomy of layer IV in cat primary auditory cortex (AI). J Comp Neurol 224:535–567.

Winer JA (1984b) Identification and structure of neurons in the medial geniculate body projecting to primary auditory cortex (AI) in the cat. Neuroscience 13:395–413.

Winer JA, Diamond IT, Raczkowski D (1977) Subdivisions of the auditory cortex of the cat: the retrograde transport of horseradish peroxidase to the medial geniculate body and posterior thalamic nuclei. J Comp Neurol 176:387–418.